Materials Science & Engineering A 717 (2018) 26–33

Contents lists available at ScienceDirect

Materials Science & Engineering A

journal homepage: www.elsevier.com/locate/msea

Microstructure and tensile behavior of friction-stir welded TRIP steel

S. Mironov[a,*], Y.S. Sato[a], S. Yoneyama[b], H. Kokawa[a,d], H.T. Fujii[a], S. Hirano[c]

[a] Department of Materials Processing, Graduate School of Engineering, Tohoku University, 6-6-02 Aramaki-aza-Aoba, Aoba-Ku, Sendai 980-8579, Japan
[b] Department of Mechanical Engineering, Aoyama Gakuin University, 5-10-1 Fuchinobe, Sagamihara 252-5258, Japan
[c] Hitachi Research Laboratory, Hitachi Ltd, 7-1-1 Omika-cho, Hitachi 319-1291, Japan
[d] School of Materials Science and Engineering, Shanghai Jiao Tong University, 800 Dongchuan Road, Minhang District, Shanghai 200240, P.R. China

ARTICLE INFO

Keywords:
Iron alloys
Plasticity methods
Phase transformations
Characterization
Electron microscopy
Stress/strain measurements

ABSTRACT

In this work, electron backscatter diffraction and digital image correlation techniques were employed to study the microstructure and microstructure-property relationship in friction-stir welded TRIP steel. It was found that the thermal effect of the welding process led to material softening in the heat-affected zone and promoted martensite transformation in the stir zone. These microstructural changes provided rapid strain localization during subsequent transverse tensile tests and thus resulted in premature failure of the welds.

Material softening in the heat-affected zone was deduced to be a combined result of dissolution and spheroidisation of retained austenite as well as recovery in bainitic ferrite. The stir zone martensite was characterized by significant orientation spread and therefore its orientation relationship with austenite essentially deviated from the ideal Kurdjumov-Sachs relation. Moreover, the martensite transformation was found to be influenced by variant selection.

1. Introduction

Transformation-induced plasticity (TRIP) steels belong to a relatively new generation of materials developed for automotive applications with the aims of weight reduction and fuel savings without compromising passenger safety, at no increased cost. The principal characteristic of such steels is the significant fraction of retained austenite. It is well known that austenite may transform to martensite upon cold deformation, thus giving rise to significant work hardening effect [1–4]. This provides a good combination of strength and ductility and hence excellent energy absorption capacity, which is required during a sudden vehicle crash.

Unfortunately, the unique microstructure of the TRIP steels is totally destroyed during conventional fusion welding and the superior properties of these materials are therefore lost. In this context, friction-stir welding (FSW), an innovative *solid-state* process [5], has recently attracted attention as a possible candidate for joining such materials.

Considering the potential advantages of this technique, several works have been undertaken recently to evaluate the effects of FSW on microstructure and mechanical properties of TRIP steels [6–9]. It was found that FSW results in complex microstructural changes. The heat input associated with the welding process induces the austenite-to-bainite phase transformation in the heat-affected zone [6,9], leading to concomitant material softening [8]. Approaching the stir zone, however, the welding temperature exceeds the A1 point, thus initiating a sequence of phase transformations that eventually lead to the formation of martensite [9]. In the stir zone, the peak temperature is believed to surpass the A3 point [8,9]. Accordingly, martensite becomes the dominant phase in this region [7–9]. However, the stir zone may also contain minor fractions of ferrite [6,8,9], bainite, and retained austenite [6–8]. These observations are explained in terms of the relatively low cooling rate during the weld thermal cycle [8,9].

The above works have significantly contributed to our current understanding of the effects of FSW on the microstructure and properties of TRIP steels. Nevertheless, several important aspects of microstructure evolution, including microstructural changes in the retained austenite and bainite as well as mechanisms of the phase transformations, remains poorly understood. This obstructs an establishment of microstructure-strength relationship. Attempting to provide deeper insight into these issues, electron backscatter diffraction (EBSD) and digital-image correlation (DIC) techniques are employed in the current study.

2. Material and experimental procedures

The material used in the present investigation was 1.2 GPa TRIP steel. The material had the nominal chemical composition listed in Table 1 and was supplied as 1.4 mm thick uncoated sheets. Thermo-

* Corresponding author.
E-mail address: S-72@mail.ru (S. Mironov).

https://doi.org/10.1016/j.msea.2018.01.053
Received 12 September 2017; Received in revised form 12 January 2018; Accepted 12 January 2018
Available online 17 January 2018

Table 1
The nominal chemical composition (wt%) of studied TRIP steel.

C	Mn	Si	Al	P	S	N	Fe
0.40	2.00	1.50	0.04	0.01	0.002	0.004	Balance

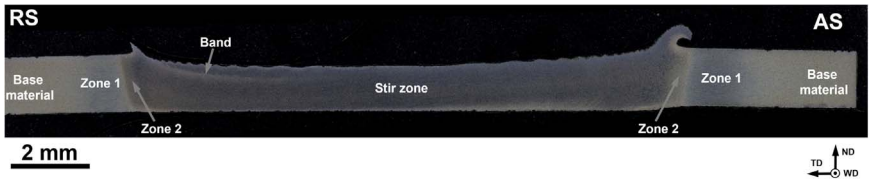

Fig. 1. Low-magnification optical image of the weld cross-section. RS and AS are the retreating side and advancing side, respectively. TD, ND, and WD are the transverse direction, normal direction, and welding direction, respectively.

Calc calculations showed that the phase transformation temperatures A1 and A3 in this material were 950 K and 1060 K, respectively. The as-received material was friction-stir welded in a bead-on-plate configuration at a tool travel speed of 60 mm/min. In an attempt to provide the lowest possible welding temperature, a relatively low tool rotational speed of 150 rpm was applied. To minimize surface oxidation, argon shielding was employed around the tool during FSW. The welding tool was fabricated from a Co-based alloy and consisted of a convex shoulder 12 mm in diameter and a 1.2 mm long probe. The probe was tapered from 5.0 mm at the shoulder to 3.0 mm at the probe tip. Further details of the tool design are shown in supplementary Fig. S1. The principal directions of the welding geometry are denoted throughout as the welding direction (WD), transverse direction (TD), and normal direction (ND).

Microstructure characterization was performed on the transverse cross-section of the weld (TD × ND plane) using optical microscopy, scanning electron microscopy (SEM), and EBSD. For optical, and SEM observations, the samples were ground with water abrasive papers, mechanically polished with 1 μm diamond finish, and chemical etched with 3% Nital. A suitable surface finish for EBSD was obtained by mechanical polishing in a similar fashion, followed by electro-polishing in 95% acetic acid + 5% perchloric acid solution at approximately 10°C–15 °C with applied potential of 40 V.

To view the microstructure distribution in the weld more broadly, the microhardness profile was measured across characteristic microstructural zones. Vickers microhardness data were obtained by applying a load of 1 kg with a dwell time of 10 s.

To assist with interpretation of the evolved microstructures, a fully-martensite structure was produced. To this end, the as-received (base) material was heated to 900 °C, soaked for 15 min, and then water quenched. Typical microstructure and microhardness distribution are shown in supplementary Fig. S2.

SEM and EBSD analyses were conducted using a Hitachi S-4300SE field-emission gun scanning electron microscope (FEG-SEM) equipped with a TSL OIM™ EBSD system and operated at accelerating voltage of 25 kV. Orientation mapping was performed using a triangular scanning grid. Depending on the particular purpose, different scan step sizes were used for mapping. Low-resolution (overview) EBSD maps were acquired using a scan step size of either 1 or 0.5 μm, whereas higher resolution maps were obtained using a scan step size of 0.2 μm. On each diffraction pattern, seven Kikuchi bands were used for indexing to minimize the possibility of misindexing errors. To ensure reliability of the EBSD data, all small grains comprising three or fewer pixels were automatically "cleaned" from the EBSD maps using the grain-dilation option of the TSL software. Furthermore, to eliminate spurious boundaries caused by orientation noise, a lower-limit boundary misorientation cut-off of 2° was used. A 15° criterion was applied to differentiate low-angle boundaries (LABs) and high-angle boundaries (HABs).

To examine mechanical behavior of the welds, transverse tensile specimens were machined. The specimens were centered at the weld line, had a gauge section 35 mm in length and 7 mm in width, and included all of the characteristic microstructural zones developed during FSW. Other details of the specimens' geometry are given in Supplementary Fig. S3. For comparative purposes, appropriate tensile specimens were also machined from the base material. Tensile tests to failure were conducted at ambient temperature and constant crosshead velocity corresponding to a nominal strain rate of $10^{-3}\,s^{-1}$ using an Instron 5969 testing machine. Five tensile specimens were tested for each material condition.

The DIC technique [10,11] was employed to evaluate strain distributions generated during the tensile tests. To this end, a random ink pattern was applied to the sample surface and a high-speed XiQMQ042MG-CM digital camera equipped with a Nikon AI AF Micro-Nikkor 200 mm f/4D IF-ED lens was used for image recording. The images were taken at a rate of 1 image per second (~ 0.1% of tensile strain). The samples for the strain distribution measurements were mechanically polished prior to the tensile tests to achieve a uniform thickness with the final polishing step comprising of 1 μm diamond.

3. Results

3.1. Microstructural observations

A low-magnification optical image of the weld cross-section is shown in Fig. 1. No volumetric defects were found but the joint exhibited evidence of bending, presumably reflecting substantial residual stresses. The optical contrast across the weld was obviously inhomogeneous, indicating complex microstructural changes induced by FSW. Five microstructural zones were defined, i.e., base material, zone 1, zone 2, stir zone, and a characteristic band region on the retreating side of the stir zone. Typical microstructures observed in these zones are summarized in Fig. 2. The brighter phase in these secondary-electron SEM images is austenite, martensite, or cementite, whereas the darker phase is ferrite (including bainitic ferrite).[1] To assist with interpretation of the microstructures, the microhardness profile was measured across these zones and the results obtained are shown in Fig. 3a.

The base material exhibited a typical ausformed microstructure with clear prior-austenite (or packet-) boundaries as well as sandwiched austenite and bainite laths arranged in blocks (Fig. 2a). The volume fraction of retained austenite was measured to be ~ 20% (Supplementary Fig. S4).

In zone 1, the austenite fraction was found to be reduced (Fig. 2b). Along with precipitation of fine cementite particles (an example is circled in Fig. 2b), this observation probably implies transformation of retained austenite to lower bainite, thus being consistent with literature data [6,9]. Moreover, nearly-equiaxed austenite particles also appeared (an example is arrowed in Fig. 2b), thus presumably reflecting a

[1] The secondary-electron contrast in SEM images is well accepted to depend on electronic structure of an irradiated material as well as from the so-called edge effect. The latter one implies that any changes in surface topography enhance emission of the secondary electrons and thus result in brighter contrast. Due to relatively high density of defects, the retained austenite and the martensite typically have more developed topography in an etched surface that the ferrite and thus they appear relatively bright.